RSC Advances

PAPER

View Article Online
View Journal | View Issue

Cite this: *RSC Adv.*, 2020, **10**, 12326

Ultra-fine platinum species supported on niobium pentoxide for CO oxidation†

Miao-Miao Wang,[ad] Jing Yu,[c] Dao-Lei Wang[e] and Rui Si *[ab]

Platinum oxide supported on a Lewis acid niobium oxide (Nb_2O_5) support has been used for various heterogeneous and homogeneous catalysts. In this work, we used urea as a precipitating agent to obtain crystallized Nb_2O_5 with high surface area *via* a hydrothermal route. Nb_2O_5-supported Pt catalysts were subsequently synthesized *via* an incipient wetness impregnation approach. Multiple characterizations including X-ray diffraction (XRD), high-resolution transmission electron microscopy (HRTEM) and nitrogen adsorption/desorption confirmed the identical structural and textural properties of the Nb_2O_5 support before and after the impregnation process. Furthermore, the X-ray absorption fine structure technique (XAFS) results with related data analysis indicate that the platinum species in the fresh and H_2-pretreated samples were in the form of single atoms or ultrafine clusters. In addition, the decrease in coordination number (CN) of the first-shell Pt–O bond, as well as the formation of Pt–Pt contribution with very low CN, after H_2-pretreatment was verified, which corresponds to the decrease of oxidation state for Pt species on the surface of supports. Thus, the ultrafine-clustered metallic Pt species are considered to be more active than the oxidized Pt single ions. The current results will be of great significance in controllable synthesis of active Pt-based catalysts for other catalytic oxidation reactions.

Received 9th February 2020
Accepted 20th March 2020

DOI: 10.1039/d0ra01252a

rsc.li/rsc-advances

1 Introduction

Platinum-based catalysts have been widely used in industry to catalyse a large number of important chemical reactions because of their superior activity and stability.[1–4] On the other hand, highly dispersed metal atoms on redox supports normally show excellent catalytic reactivity in various reactions by means of maximizing the efficiency of active metal atoms.[5–7] Therefore, more and more research groups have shown that sub-nanosized clusters or single atoms exhibit better catalytic performance than nanosized metal or metal oxide particles.[8–14] Judai *et al.* confirmed that the cluster catalysts consisting of only a few Pd atoms are active at much lower temperature than the bulk analogues for the NO reduction by CO.[9] The Zhang group synthesized isolated single Pt atoms anchored onto iron oxide (FeO_x), which exhibited very high activity and stability for both CO oxidation and preferential oxidation (PROX) of CO.[11]

Other research results have shown that increasing the surface area of the supports can effectively improve dispersion to optimize activity.[15] The pretreatment of the catalysts by specific gas can also disperse the active metal particles thereby increasing catalytic activity. For instance, The Qin group used HCl steam to re-disperse Pt nanoparticles in process of propane dehydrogenation for better catalytic activity.[13] Original large-sized Mo oxide on carbon support was calcined in an H_2 atmosphere for obtaining small-sized Mo species.[16] After vacuum calcination and H_2 reduction, thermal treatment of 0.2 wt% Pt/SiO_2 was used to synthesize Pt particles less than 1 nm that are uniformly dispersed on the SiO_2.[17] At present, some researchers on the evolution of single-atom catalysts (SACs) during activation and catalytic reactions show that ultrafine cluster is more active than pure single atoms. Recently, Piccolo Group demonstrated the importance of Pt clusters for CO oxidation reaction by means of *in situ* characterization methods.[18] Pt–O–Pt sites, represented by a Pt_8O_{14} model cluster were built on ceria for low-temperature CO oxidation reaction, which is 100–1000 times more active than their single atom Pt_1/CeO_2 parent.[19]

Many oxides (Al_2O_3,[18,20–22] Fe_3O_4,[23,24] Co_3O_4,[25,26] ZrO_2,[22,27] and, MnO_2,[28,29] *etc.*) were applied to support Pt for various heterogeneous catalytic reactions. Among them, niobium oxide (Nb_2O_5) has been used as a solid acid catalyst with the Lewis acid sites on its surface for various heterogeneous or homogeneous catalysis.[15,30–38] Oxygen vacancies were introduced into Nb_2O_5 *via* thermal treatment to obtain defective Nb_2O_5-supported Pt catalysts for CO oxidation.[36] So, niobium pentoxide supported platinum metal catalyst may be a promising catalyst.

[a]*Shanghai Institute of Applied Physics, Chinese Academy of Sciences, Shanghai, 201204, Shanghai, China. E-mail: sirui@sinap.ac.cn*
[b]*Shanghai Synchrotron Radiation Facility, Zhangjiang Laboratory, Shanghai, 201204, Shanghai, China*
[c]*Shanghai Institute of Measurement and Testing Technology, Shanghai 200233, China*
[d]*University of Chinese Academy of Science, Beijing 100049, China*
[e]*Division of China, TILON Group Technology Limited, Shanghai 200090, China*

† Electronic supplementary information (ESI) available. See DOI: 10.1039/d0ra01252a

However, present published results had limited research about Pt-based Nb_2O_5 catalysts for heterogeneous catalysis, especially for CO oxidation reactions.

In this work, we used urea as a precipitating agent to obtain pure-phase Nb_2O_5 with high specific surface area by hydrothermal method using niobium(v) oxalate hydrate as a precursor and loaded different amounts of Pt species *via* incipient wetness impregnation subsequently. The catalytic activity of catalysts were tested *via* the CO oxidation reaction which is a typical benchmark reaction for estimating catalysts and plays a pivotal role in catalysis for both fundamental research and industrial applications,[34,39–41] including purification of polluted gases, preferential removal of CO in proton exchange membrane fuel cells under hydrogen-rich conditions, CO gas sensors and CO elimination of automotive exhaust gases. Our results indicate that the method of preparing Nb_2O_5 can effectively disperse and anchor Pt atoms due to high specific surface area (127 $m^2\ g^{-1}$) of the Nb_2O_5 compared to that of other reports (10 $m^2\ g^{-1}$–65 $m^2\ g^{-1}$).[32–34,36] In the case of Pt-based catalysts, the pretreatment with H_2 of the catalysts was to reduce the platinum species for obtaining reduced platinum which is active species for CO oxidation. But X-ray absorption fine structure (XAFS) analysis results of this work indicated the increase of catalyst activity after hydrogen pretreatment is not only due to the decrease of the oxidation state for Pt species but also to the appearance of Pt fine-clusters on the surface of supports.

2 Materials and methods

2.1 Materials

All the chemicals are analytical grade and were used without further purified and modified. Urea ($CO(NH_2)_2$, ≥ 99.0%) was purchased from Sinopharm Chemical Reagent Co., Ltd. Tetraammineplatinum(II) nitrate ($Pt(NH_3)_4(NO_3)_2$, 99.99%) and niobium(v) oxalate hydrate powder was purchased from Alfa Aesar Chemical Reagent Co., Ltd.

2.2 Catalyst preparation

Preparation of Nb_2O_5 supports. 2.402 ± 0.001 g of urea and 4.304 ± 0.001 g of niobium(v) oxalate hydrate powder (molar ratio, $CO(NH_2)_2$: Nb = 10 : 1) was dissolved in 20 mL of deionized and 60 mL of deionized water at room temperature, respectively. The mixed solution was transferred to a Teflon-lined stainless-steel autoclave (inner volume: 100 mL) and then heated at 80 °C for 8 hours in vessel. And the temperature was sequentially elevated up to 200 °C and kept for two days. After the hydrothermal process finished and the vessel was cooled down to room temperature, the resulting precipitate was isolated by centrifugation, washed repeatedly with deionized water until neutral. The as-washed products were dried at 80 °C overnight and then calcined at 400 °C for 4 h at muffle furnace. After grinding and sieving (100 mesh) the calcined samples, the Nb_2O_5 fresh powder was obtained with the white colour.

Preparation of Pt/Nb_2O_5 samples. The deposition of platinum onto the Nb_2O_5 supports was obtained by incipient wetness impregnation (IMP). The atomic percentage of Pt was designed to be 0.05, 0.1, 0.3, 0.5 and 1.0 at%, which was denoted as 0.05 Pt/Nb_2O_5, 0.1 Pt/Nb_2O_5, and 0.3 Pt/Nb_2O_5, 0.5 Pt/Nb_2O_5 and 1.0 Pt/Nb_2O_5, respectively. After the impregnation step, the catalysts were dried at 80 °C for 12 h and then calcined at 400 °C for 4 h under static air in a muffle furnace.

2.3 Characterization

Transmission electron microscope (TEM). All the tested samples were suspended fully in ethanol and then dropped on an ultrathin carbon stainless-steel Mo grid. The prepared samples were dried naturally under ambient conditions before placed on the TEM sample holder. The transmission electron microscopy, high-resolution transmission electron microscopy (HRTEM) images were obtained from a FEI Tecnai G2 F20 microscope (FEI Co., Hillsboro, TX, USA) operating at 200 kV with a Genesis XM2 accessory (EDAX Inc., Mahwah, NJ, USA).

X-ray diffraction. The grinded catalyst was placed inside a quartz-glass sample holder and flattened before each testing. X-ray diffraction was carried out on a Bruker AXS D2 PHASER, using Cu Kα radiation (λ = 0.15406 nm). The diffraction patterns were collected from 10 to 90° with a step of 0.02°. The 2θ angles were calibrated with a micrometer-scale alumina disc.

X-ray absorption fine structure (XAFS). The XAFS spectra at Pt L3-edge (E_0 = 11 564.0 eV) were performed at BL14W1 beamline of the Shanghai Synchrotron Radiation Facility (SSRF) operated at 3.5 GeV under "top-up" mode with a constant current of 220 mA. The sample mixing LiF uniformly was pressed into a sheet, then sealed with Kapton tape before the XAFS test. The XAFS data were recorded under fluorescence mode with a standard Lytle ion chamber. The energy was calibrated with Pt foil as a reference. Athena and Artemis codes were used to extract the data and fit the profiles. For the X-ray absorption near-edge spectroscopy (XANES) part, the experimental absorption coefficients as function of energies $\mu(E)$ were processed by background subtraction and normalization procedures and reported as "normalized absorption". Based on the normalized XANES profiles, both the molar proportion of Pt^{4+}/Pt^0 and the oxidation state of Pt can be determined by the linear combination fit with the help of various references (Pt foil for Pt^0 and PtO_2 for Pt^{4+}). For the extended X-ray absorption fine structure (EXAFS) part, the Fourier transformed (FT) data in R space were analysed by applying PtO_2 and metallic Pt model for Pt–O and Pt–Pt contributions. The passive electron factors, S_0^2, were determined by fitting the experimental data on Pt foils and setting the coordination number (CN) of Pt–Pt to be 12, and then fixed for further analysis of the measured samples. The parameters describing the electronic properties (*e.g.*, correction to the photoelectron energy origin, E_0) and local structure environment including CN, bond distance (R), and Debye–Waller factor around the absorbing atoms (σ^2) were allowed to vary during the fit process. The fitted ranges for K and R spaces were selected to be k = 2.5–11.8 $Å^{-1}$, 2.5–10.5 $Å^{-1}$, 2.5–8.0 $Å^{-1}$, 2.5–12.0 $Å^{-1}$, 2.5–8.5 $Å^{-1}$ or 2.5–12.0 $Å^{-1}$ for 1 Pt/Nb_2O_5-fresh, 1 Pt/Nb_2O_5–H_2, 1 Pt/Nb_2O_5-used, 0.3 Pt/Nb_2O_5-fresh, 0.3 Pt/Nb_2O_5–H_2, 0.3 Pt/Nb_2O_5-used, respectively.

Nitrogen adsorption–desorption. For testing the BET specific surface area and pore size distribution of the samples, the nitrogen adsorption–desorption characterization was performed on an ASAP2020-HD88 analyzer (Micromeritics Co., Ltd., Atlanta, GA, USA) at 77 K. The fresh powders were degassed at 250 °C under vacuum over 4 h and then analysed under N_2 atmosphere cooling with liquid nitrogen. The BET specific surface areas (S_{BET}) were obtained from data of the relative pressure between 0.05 and 0.20.

Inductively coupled plasma atomic emission spectroscopy (ICP-AES). The platinum concentrations were examined by ICP-AES on Optima 5300DV (PerkinElmer corp.)

H_2-temperature programmed reduction (H_2-TPR). H_2-TPR measurement of the samples was performed on micromeritics AutoChem 2920 equipped with a thermal conductivity detector (TCD) to detect H_2 consumption. Before measurement, the fresh sample (50 mg, 20–40 mesh) was pretreated in 5% O_2/Ar (30 mL min^{-1}) at 300 °C for 30 min. After cooling down, the measured sample was heated from room temperature to 600 °C with a step of 10 °C min^{-1} in continuous 5% H_2 with He as balance gas.

2.4 Catalytic test

CO oxidation reactions were carried out in micromeritics AutoChem 2920. The detection processes of catalyst activity were as follows: The sieved sample (40–60 mesh, 50 mg) was loaded into a U-shaped quartz tube, and then preactivated at 5% H_2/95% He or 5% O_2/95% N_2 for 30 min with a flow rate of 50 mL min^{-1} before the reaction. After the reactor cooled to room temperature, pure He gas was used to purge H_2 or O_2 for 20 minutes. Afterwards, CO oxidation activities of Pt/Nb_2O_5 catalysts were measured in a stoichiometric gas mixture of 2% CO/1% O_2/97% He at a flow rate of 30 mL min^{-1}, corresponding to a gas hourly space velocity (GHSV) of 36 000 mL h^{-1} $g_{cat}{}^{-1}$. The reactant temperature began from 30 °C to 300 °C with the heating rate of 10 °C min^{-1} and the outlet gas compositions of CO and CO_2 were recorded on-line at 30 °C per step by Micro GC fusion gas chromatography (INFICON company). The CO conversion of CO oxidation was calculated according to the following equation: CO conversion (%) = $(CO_{in} - CO_{out})/CO_{in} \times 100$. The experimental error is within 3%.

3 Results and discussion

3.1 Catalytic performance of Pt/Nb_2O_5 catalysts for CO oxidation reaction

CO oxidation reaction, as model catalysis reaction, was used to evaluate the catalytic performance of platinum-doped Nb_2O_5 catalysts. Fig. 1a and b show the "light-off" profiles of H_2-pretreated and O_2-pretreated samples, respectively, which display that all the Pt/Nb_2O_5 samples exhibited CO conversions. In addition, this figure shows that CO conversion increases with elevating Pt content and the catalysts pretreated with H_2 exhibit improved activity whereas the ones pretreated with O_2 exhibit worse activity. At 50% conversion of the same component, the conversion temperature of the samples after H_2-pretreatment is

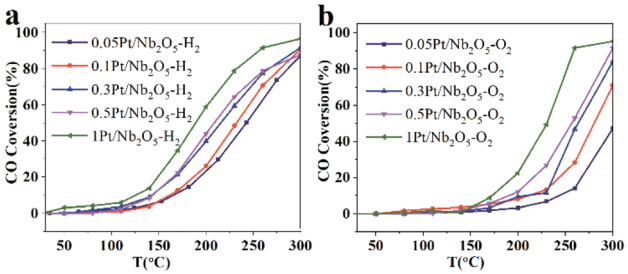

Fig. 1 CO oxidation conversion over Pt–Nb_2O_5 samples for "light-off" experiments from 30 to 300 °C of catalysts.

about 40 °C to 50 °C lower than the conversion temperature of the oxygen pretreated samples (Table 1). For example, the temperature of 50% CO conversion is 231 °C for O_2-pretreated 1% Pt catalysts, but 189 °C for H_2-pretreated 1% Pt catalysts. Similarly, the temperature of 50% CO conversion is 265 °C for O_2-pretreated 0.3% Pt catalysts, but 215 °C for H_2-pretreated 0.3% Pt catalysts. This result implies that Pt species with low valence are more effective than Pt species with high valence for CO oxidation.[19,42] Further reasons are explored in the following characterization. Recently, Tran *et al.* reported about 50% CO oxidation at 160 °C under 60 000 mL g^{-1} h^{-1} over 4 wt% Pt/Nb_2O_5 under 2% CO/5% O_2/He.[36] CO oxidation activities of Pt/Nb_2O_5 catalysts were measured in a stoichiometric gas mixture of 2% CO/1% O_2/97% He corresponding to a gas hourly space velocity (GHSV) of 36 000 mL h^{-1} $g_{cat}{}^{-1}$ in this work. Considering the Pt content and the oxygen enrichment conditions in that work, the reactivity of our catalyst is competitive.

3.2 Structural and textural properties of Pt/Nb_2O_5 catalysts

XRD was performed to determine the crystal structure of platinum-doped niobium oxide catalysts. The XRD patterns in Fig. S1a† identify that Pt-free Nb_2O_5 sample presented a pseudo-hexagonal structure (JCPDS card no: 28-317) with TT phase.[43] In addition, no Pt-containing peaks were identified for all fresh catalysts shown in Fig. S1a.† 1 Pt and 0.3 Pt catalysts were selected for hydrogen pretreatment and further XRD testing (Fig. S1b†). There are no Pt peaks on H_2-pretreated catalysts, which preliminarily indicates the high dispersion or small size of Pt species. As for used samples, no Pt species are found for all samples (see Fig. S2a and b†). The average crystallite size calculated by the Scherrer equation for pure Nb_2O_5 is 11.9 nm (see Table 2). Crystallite sizes of niobium pentoxide with hexagonal structure synthesized using solvent evaporation method were 61.4 nm in Ziolek' work.[32] Table 2 shows that the average crystallite size is between 10.4 and 14.9 nm for all the investigated fresh catalysts, H_2-pretreated and used samples after CO oxidation according to the results of XRD calculated by the Scherrer equation, which indicating that contents of Pt and pretreatment conditions have no clear effect for the Nb_2O_5 support. (001) and (100) peaks of the XRD of the used samples were selected to plot the intensity seen in Fig. S3.† There is no obvious evidence to prove the regular development of materials with hydrogen pretreatment or oxygen pretreatment, as

Table 1 Pt concentration, BET specific surface areas (S_{BET}), BJH pore volume (V_p) of Nb_2O_5 supports, temperature for 50% CO conversion ($T_{1/2}$)

Sample	Pt loading[a] (at%)	S_{BET}[b] ($m^2\ g^{-1}$)	V_p[b] ($cm^3\ g^{-1}$)	$T_{1/2}$[c] (°C)
Nb_2O_5	—	127 ± 1	0.296 ± 0.002	—
1 Pt–Nb_2O_5	0.8	121 ± 1	0.280 ± 0.002	231[d] 189[e]
0.5 Pt–Nb_2O_5	0.4	120 ± 1	0.287 ± 0.003	258[d] 209[e]
0.3 Pt–Nb_2O_5	0.3	121 ± 1	0.290 ± 0.002	265[d] 215[e]
0.1 Pt–Nb_2O_5	0.1	119 ± 1	0.289 ± 0.002	282[d] 233[e]
0.05 Pt–Nb_2O_5	0.07	114 ± 1	0.280 ± 0.003	>300[d] 244[e]

[a] Determined by ICP. [b] From N_2 adsorption/desorption. [c] Temperature for 50% CO conversion. [d] After O_2-pretreatment. [e] After H_2-pretreatment.

mentioned above. A series of Pt/Nb_2O_5 samples prepared using $NbCl_5$ as a precursor shown crystal size of 45–54 nm reported by Tran *et al.*[36] These comparative data are indication that the successful precipitation of niobium ions *via* urea to obtain small nanosized Nb_2O_5 support in this work.

Summarizing the results of XRD analysis, the fresh catalysts, the H_2-pretreated samples and the used samples are not observed peaks related to platinum structure due to the ultra-fine sizes or high dispersion of platinum species.

The ICP-AES results (see Table 1) show that the experimental Pt content is close to the target value for each catalyst. N_2 adsorption–desorption results are present in Fig. S4† and summarized in Table 1. Both Nb_2O_5 support and Pt–Nb_2O_5 catalysts show type IV adsorption isotherm and H1-type hysteresis loop with the BJH pore volumes (*V*p) between 0.280–0.296 $cm^3\ g^{-1}$. Also, the surface area was almost the same after Pt deposition (114–121 $m^2\ g^{-1}$), indicating the good support of nanosized Nb_2O_5 for platinum. Furthermore, a particularly high BET specific surface area (127 $m^2\ g^{-1}$) was determined for Nb_2O_5, which provides a matrix for Pt loading in this work. All these data indicate that the introduction of Pt species has no significant effect on the textural properties of Nb_2O_5, and Pt–Nb_2O_5 catalysts were stable after air-calcination at 400 °C.

For further analysis, the Nb_2O_5, 0.3 Pt/Nb_2O_5 and 1 Pt/Nb_2O_5 samples were subjected to TEM characterization. The TEM images of pure Nb_2O_5 support in Fig. 2a show a worm-like aggregation with a primary particle size of about 11 nm (see Table 2), which is consistent with the XRD results. The HRTEM image in Fig. 2b clearly displays an interplanar spacing of

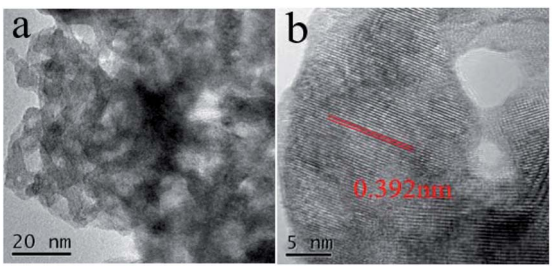

Fig. 2 TEM images of Nb_2O_5 samples.

Table 2 Averaged Grain Size (D_{XRD}) and Particle Size (D_{TEM}) of samples

	D_{XRD}[a] (nm)			D_{TEM}[b] (nm)		
Sample	Fresh[c]	H_2[d]	Used[e]	Fresh[c]	H_2[d]	Used[e]
Nb_2O_5	11.9	—	—	11.3 ± 2.4	—	—
1 Pt–Nb_2O_5	14.9	12.5	13.5[f] 10.8[g]	12.4 ± 2.6	12.1 ± 1.9	13.1 ± 2.3[f]
0.5 Pt–Nb_2O_5	11.7	—	9.6[f] 13.7[g]	—	—	—
0.3 Pt–Nb_2O_5	13.3	12.5	10.8[f] 11.4[g]	11.2 ± 2.8	11.7 ± 2.5	11.1 ± 3.1[f]
0.1 Pt–Nb_2O_5	12.6	—	13.4[f] 12.4[g]	—	—	—
0.05 Pt–Nb_2O_5	10.4	—	10.7[f] 10.7[g]	—	—	—

[a] Calculated from XRD patterns by Scherrer equation. [b] Statistic data on the basis of TEM images. [c] Fresh samples. [d] After H_2-pretreatment. [e] Used samples after CO oxidation. [f] After CO oxidation with H_2-pretreatment. [g] After CO oxidation with O_2-pretreatment.

0.392 nm, corresponding to the (001) lattice fringe of pseudo-hexagonal Nb_2O_5. No metallic Pt particles but the only structure of Nb_2O_5 was observed in HRTEM for both 0.3 Pt/Nb_2O_5 (Fig. 3a) and 1 Pt/Nb_2O_5 (Fig. 3b). Similarly, the HRTEM images of the H_2-pretreated samples and used samples shown in Fig. 3c–f also show no Pt species. Clearly visible lattice fringes appearing on all images belong to the (001) crystal plane of Nb_2O_5. STEM-EDS mapping of fresh 1 Pt/Nb_2O_5 and used 0.3 Pt–Nb_2O_5 with H_2-pretreatment are shown in Fig. S5,† which indicates that Pt is uniformly dispersed on the support, but size and form of Pt are still unclear. Consulting other groups' work about Pt/Nb_2O_5, Pt species were loaded on Nb_2O_5 with size of particles of 2.7–17.9 nm,[30,31,36,44] while the Pt species of calcined samples in this work cannot be identified on HRTEM images, suggesting that ultrafine Pt species supported in Nb_2O_5 obtained by the urea-based deposition–precipitation approach, proving the superiority of nanosized Nb_2O_5 in this work.

The results of this part are briefly summarized: Nb_2O_5 nanocrystalline obtained by the urea-based deposition–precipitation approach is thermally stable. XRD and HRTEM characterization revealed that the deposited Pt species on Nb_2O_5 are extremely small.

3.3 Reducibility and active species of Pt/Nb_2O_5 catalysts

Fig. 4 shows the H_2-TPR profiles of the as-calcined samples. On the one hand, the TPR of the Nb_2O_5 support results in no reduction peak between 30 and 500 °C, confirming that no surface reduction of the support takes place without Pt. On the other hand, the two small reduction peaks for Nb_2O_5-supported Pt samples were observed with the peaks at 61 °C and 331 °C. The former reduction peak suggested a reduction of surface Pt oxide to metallic platinum.[36,44] And the latter reduction peak showed that the reduction of surface lattice oxygen related to the metal oxide support interacting with Pt species.[36,45,46]

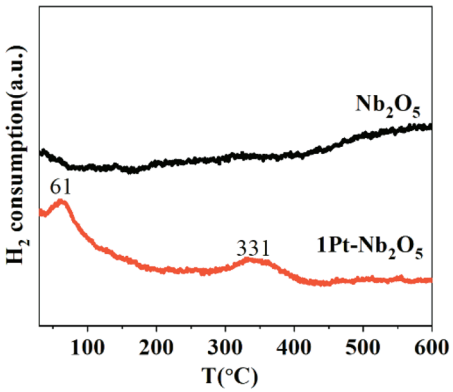

Fig. 4 H_2-TPR analysis of the synthesized catalysts.

Since no peaks of Pt species could be observed from XRD and about the size and dispersion of Pt species could not be obtained from HRTEM. For further research, XAFS was used to study the electronic and the local coordination structure of the 1 Pt/Nb_2O_5 and 0.3 Pt/Nb_2O_5. The XANES data for Pt L3-edge in Fig. 5a and b clearly demonstrate that the white line peaks of samples are all between Pt foil and PtO_2 but closer to Pt foil, indicating that the low valence state of Pt in fresh samples and H_2-pretreatment samples. By means of the linear combination Pt/Nb_2O_5 fresh sample and the 1 Pt/Nb_2O_5 fresh sample are 1.82 (Table 3). However, the valence states of Pt in the H_2-pretreated

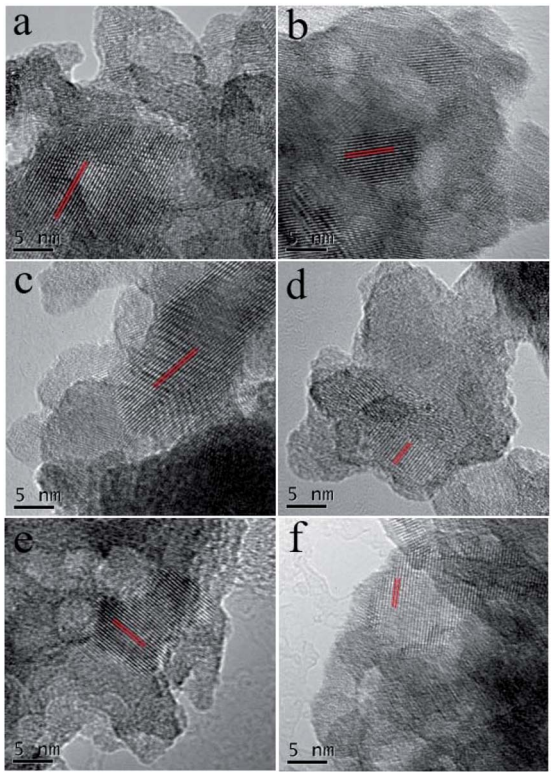

Fig. 3 HRTEM images of (a, c and e) 0.3 Pt/Nb_2O_5 and (b, d and f) 1 Pt/Nb_2O_5; (a and b) fresh samples; (c and d) after H_2-pretreatment samples; (e and f) used samples with H_2-pretreatment samples.

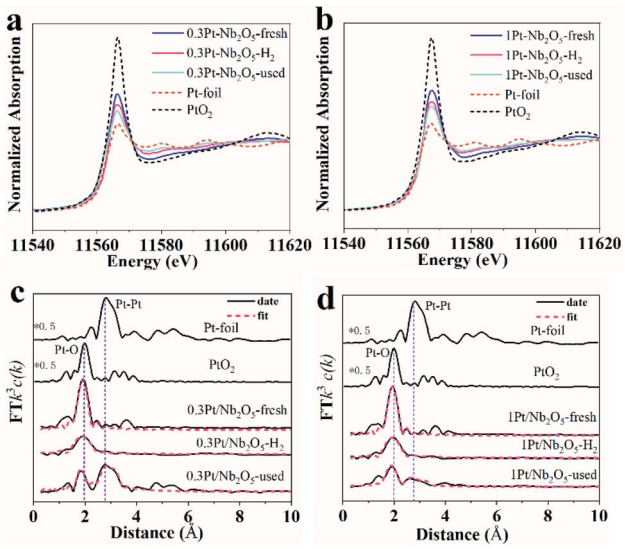

Fig. 5 Pt L3-edge XANES profiles (a and b) and EXAFS fitting results in R space (c and d) of Pt–Nb_2O_5 samples: (a and c) 0.3 Pt–Nb_2O_5 and (b and d) 1 Pt–Nb_2O_5.

Table 3 Oxidation state of platinum (δ) and Pt L3-edge EXAFS fitting results (R, distance; CN, coordination number; σ^2 Debye–Waller factor; ΔE_0, inner potential correction b) of Pt–Nb_2O_5 samples

		Pt–O		Pt–Pt			
Sample	δ	R (Å)	CN	R (Å)	CN	σ^2 (Å^2)	ΔE_0 (eV)
1 Pt–Nb_2O_5-fresh	1.82 ± 0.04	1.98 ± 0.01	4.1 ± 0.2	—	—	0.003(O)0.005 ± 0.001(Pt)	12.1 ± 0.7
1 Pt–Nb_2O_5–H_2	1.20 ± 0.02	2.00 ± 0.01	2.2 ± 0.2	—	—		10.2 ± 2.5
1 Pt–Nb_2O_5-used	1.01 ± 0.02	1.97 ± 0.01	1.9 ± 0.2	2.70 ± 0.02	1.8 ± 0.6		8.3 ± 1.4
0.3 Pt–Nb_2O_5-fresh	1.84 ± 0.02	1.98 ± 0.01	4.1 ± 0.3	—	—		12.1 ± 0.7
0.3 Pt–Nb_2O_5–H_2	1.13 ± 0.02	2.00 ± 0.02	2.3 ± 0.5	—	—		10.2 ± 2.5
0.3 Pt–Nb_2O_5-used	0.72 ± 0.02	1.97 ± 0.01	1.7 ± 0.3	2.74 ± 0.01	4.9 ± 1.2		8.3 ± 1.4

samples is reduced, that for 0.3 Pt/Nb_2O_5 sample and the 1 Pt/Nb_2O_5 sample are 1.20 and 1.13, respectively. Obviously, the supported Pt were reduced partially by the hydrogen. As for used samples with H_2-pretreatment, the valence of Pt is further reduced compared to the H_2-pretreated samples for both of 0.3 Pt/Nb_2O_5 and 1 Pt/Nb_2O_5, which evidently shown in Fig. 5a, b and Table 3.

The related EXAFS spectra of Pt L3-edge exhibit a single prominent peak at *ca.* 1.98 Å originating from the first shell of Pt–O contribution with a coordination number (CN) of around 4.1 (see Table 3) for both of 0.3 Pt/Nb_2O_5 fresh sample (Fig. 5c) and 1 Pt/Nb_2O_5 fresh sample (Fig. 5d), which strongly indicate that Pt species exist with the form of single atoms for calcined samples. After hydrogen pretreatment, according to the results of the fitting, only the Pt–O shell was found without the peak of the Pt–Pt shell because the second shell is too small to fitted. But the existence of ultrafine clusters cannot be denied and neglected because there are very small peak corresponding to the Pt–Pt shell in Fig. 5c and d for 0.3 Pt/Nb_2O_5 and 1 Pt/Nb_2O_5. It is worth noting that the intensity of Pt–O peak of H_2-pretreated catalysts significantly decline compared to fresh samples, accompanied by considerable decrease of coordination number (4.1 to 2.2 for 1 Pt and 4.1 to 2.3 for 0.3 Pt) and slight extension of Pt–O bond (1.98 Å to 2.00 Å for both of them), and the second shell Pt–Pt is very inconspicuous, which indicates that some single atoms formed to ultrafine clusters during H_2-pretreatment. In other words, H_2-pretreatment promotes a few of single atoms to form ultrafine clusters on the surface of the Nb_2O_5 resulting in higher activity for CO oxidation than O_2-pretreatment catalysts. For the used samples, the very obvious Pt–Pt shell (2.70 Å for 1 Pt and 2.74 Å for 0.3 Pt) appeared with high CN that is 1.8 and 4.9 for 1 Pt and 0.3 Pt respectively besides the Pt–O shell seen Fig. 5c and d, which show that bigger Pt clusters were formed on used samples.

3.4 Discussion

There are no characteristic peaks of Pt species on the XRD patterns (Fig. S1 and S2†) of the all Pt-based catalysts. 0.3 Pt–Nb_2O_5 and 1 Pt–Nb_2O_5 samples after CO oxidation with H_2-pretreatment were chosen to be characterized by TEM. The TEM images are not available for obtaining the information of Pt species of the used samples because the size of Pt species is less than the limit of detection of the device, which indicates that no Pt nanoparticles were formed after the reaction. TEM also shows no structural transformation on supports for H_2-pretreatment and used catalysts compared with fresh samples. All the above analysis shows that catalyst supports have no obvious deformation or aggregation during reaction test, so the catalysts are very stable during the CO reaction.

H_2-TPR confirmed the interaction between the Pt species and Nb_2O_5 because the pure support did not exhibit the reduction peak of the surface lattice oxygen in 331 °C in the test temperature range, while it appeared after the loading of Pt. It should be noted that since the low-content catalysts do not easily exhibit peaks in H_2-TPR, only the spectrum of the 1 Pt catalyst is shown here.

The most important information about explanation of the above phenomenon is derived from XAFS results undoubtedly. Comparing the XAFS spectrum and analytical results of the H_2-pretreated catalysts and the as-prepared catalysts, the H_2-pretreated samples possess a tiny peak belonging to the Pt–Pt shell that is absent for fresh catalysts. The only one Pt–O shell for fresh catalysts sufficiently indicate that Pt species exist in the form of single atoms, which illustrates the success of the synthetic method of Nb_2O_5. The lower valence of Pt after H_2-pretreatment accounts for higher activity of CO conversion corresponding to the "light-off" curves of the CO oxidation reaction, which confirmed by the works of other research groups.[19,42] Then, decrease of coordination number and slight extension of Pt–O bond after H_2-pretreatment and the appearance of Pt–Pt shell, which indicates H_2-pretreatment process promotes a few of single atoms to form ultrafine Pt clusters on the Nb_2O_5 surface resulting in higher activity than O_2-pretreatment catalysts. We hypothesize the similar local coordination structure for O_2-pretreated catalysts and the fresh catalysts because the fresh catalysts were obtained by calcination in air. Therefore, the above conclusions obtained by analysing and comparing the XAFS results of fresh catalysts and H_2-pretreated catalysts are reliable and reasonable. XAFS reveals more details about the used catalysts. The used samples produce Pt–O shell and Pt–Pt shell according to the fitting results (see Fig. 5 and Table 3). At the same time, the coordination number of Pt–O shell for used samples decreased (3.9–1.2 Å for 1 Pt–Nb_2O_5 and 4.2–1.6 Å for 0.3 Pt–Nb_2O_5) compared to H_2-pretreat samples. It indicates that the coordination environment of Pt species undergone dramatic changes during the reaction. In other words, ultrafine Pt clusters form bigger Pt clusters during CO

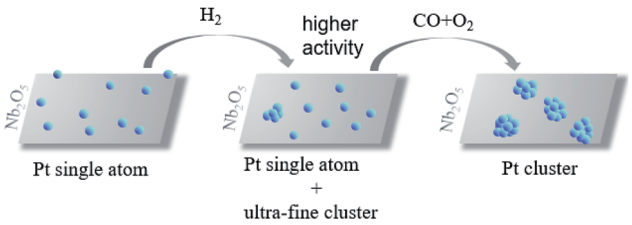

Scheme 1 Schematic illustration of the structural transformation of Pt/N_2O_5.

oxidation reaction. The structural transformation of Pt/N_2O_5 is shown in Scheme 1.

4 Conclusions

Nb_2O_5 with a high surface area was obtained by the hydrothermal method using urea as a precipitating agent and different content Pt/Nb_2O_5 catalysts were synthesized *via* incipient wetness impregnation. XAFS, a powerful tool for exploring the relationship between catalyst structure and structure-activity, indicates that Pt species present in fresh and H_2-pretreated catalysts with the form of single atoms and fine clusters even when the content of Pt is 1%. The reasons for higher catalyst activity after H_2-pretreated catalysts than O_2-pretreated is not only due to the reduction of the valence state of Pt species but also to the appearance of Pt fine-clusters on the surface of supports according to XAFS spectrum and its corresponding analysis results. The current results will be of great significance in controllable synthesis of active ultrafine clusters or single atom Pt-based catalysts for other catalytic oxidation reactions.

Conflicts of interest

There are no conflicts to declare.

Acknowledgements

Financial supported from the National Science Foundation of China (NSFC) (grant no. 21773288) and the National Key Basic Research Program of China (2017YFA0403402).

Notes and references

1 P. Gélin and M. Primet, *Appl. Catal., B*, 2002, **39**, 1–37.
2 L. V. Mattos and F. B. Noronha, *J. Power Sources*, 2005, **145**, 10–15.
3 C. Zhou, H. Wang, F. Peng, J. Liang, H. Yu and J. Yang, *Langmuir*, 2009, **25**, 7711–7717.
4 K. An, S. Alayoglu, N. Musselwhite, S. Plamthottam, G. Melaet, A. E. Lindeman and G. A. Somorjai, *J. Am. Chem. Soc.*, 2013, **135**, 16689–16696.
5 M. Haruta, *Catal. Today*, 1997, **36**, 153–166.
6 Y. Lei, F. Mehmood, S. Lee, J. Greeley, B. Lee, S. Seifert, R. E. Winans, J. W. Elam, R. J. Meyer, P. C. Redfern, D. Teschner, R. Schlogl, M. J. Pellin, L. A. Curtiss and S. Vajda, *Science*, 2010, **328**, 224–228.
7 J. Jones, H. Xiong, A. T. DeLaRiva, E. J. Peterson, H. Pham, S. R. Challa, G. Qi, S. Oh, M. H. Wiebenga, X. I. Pereira Hernandez, Y. Wang and A. K. Datye, *Science*, 2016, **353**, 150–154.
8 M. Valden, *Science*, 1998, **281**, 1647–1650.
9 K. Judai, S. Abbet, A. S. Wörz, U. Heiz and C. R. Henry, *J. Am. Chem. Soc.*, 2004, **126**, 2732–2737.
10 M. Turner, V. B. Golovko, O. P. H. Vaughan, P. Abdulkin, A. Berenguer-Murcia, M. S. Tikhov, B. F. G. Johnson and R. M. Lambert, *Nature*, 2008, **454**, 981–983.
11 B. Qiao, A. Wang, X. Yang, L. F. Allard, Z. Jiang, Y. Cui, J. Liu, J. Li and T. Zhang, *Nat. Chem.*, 2011, **3**, 634–641.
12 L. Wang, H. Li, W. Zhang, X. Zhao, J. Qiu, A. Li, X. Zheng, Z. Hu, R. Si and J. Zeng, *Angew. Chem.*, 2017, **129**, 4790–4796.
13 J. Liu, C. Liu, A. Ma, J. Rong, Z. Da, A. Zheng and L. Qin, *Appl. Surf. Sci.*, 2016, **368**, 233–240.
14 M. Moses-DeBusk, M. Yoon, L. F. Allard, D. R. Mullins, Z. Wu, X. Yang, G. Veith, G. M. Stocks and C. K. Narula, *J. Am. Chem. Soc.*, 2013, **135**, 12634–12645.
15 T. Murayama, W. Ueda and M. Haruta, *ChemCatChem*, 2016, **8**, 2620–2624.
16 J. Chen, H. Wang, Z. Wang, S. Mao, J. Yu, Y. Wang and Y. Wang, *ACS Catal.*, 2019, **9**, 5302–5307.
17 H. Wang, J.-X. Liu, L. F. Allard, S. Lee, J. Liu, H. Li, J. Wang, J. Wang, S. H. Oh, W. Li, M. Flytzani-Stephanopoulos, M. Shen, B. R. Goldsmith and M. Yang, *Nat. Commun.*, 2019, **10**, 3808.
18 C. Dessal, T. Len, F. Morfin, J.-L. Rousset, M. Aouine, P. Afanasiev and L. Piccolo, *ACS Catal.*, 2019, **9**, 5752–5759.
19 H.-C. Wu, T.-C. Chen, Y.-C. Chen, J.-F. Lee and C.-S. Chen, *J. Catal.*, 2017, **355**, 87–100.
20 A. S. Chellappa, C. M. Fischer and W. J. Thomson, *Appl. Catal., A*, 2002, **227**, 231–240.
21 A. S. Ivanova, E. M. Slavinskaya, R. V. Gulyaev, V. I. Zaikovskii, O. A. Stonkus, I. G. Danilova, L. M. Plyasova, I. A. Polukhina and A. I. Boronin, *Appl. Catal., B*, 2010, **97**, 57–71.
22 F. Pompeo, N. N. Nichio, M. M. V. M. Souza, D. V. Cesar, O. A. Ferretti and M. Schmal, *Appl. Catal., A*, 2007, **316**, 175–183.
23 P. Zhang, R. Li, Y. Huang and Q. Chen, *ACS Appl. Mater. Interfaces*, 2014, **6**, 2671–2678.
24 C. Wang, H. Daimon and S. Sun, *Nano Lett.*, 2009, **9**, 1493–1496.
25 Z. Jiang, X. Feng, J. Deng, C. He, M. Douthwaite, Y. Yu, J. Liu, Z. Hao and Z. Zhao, *Adv. Funct. Mater.*, 2019, **29**, 1902041.
26 Z. Yan, Z. Xu, B. Cheng and C. Jiang, *Appl. Surf. Sci.*, 2017, **404**, 426–434.
27 D.-W. Jeong, H. S. Potdar, J.-O. Shim, W.-J. Jang and H.-S. Roh, *Int. J. Hydrogen Energy*, 2013, **38**, 4502–4507.
28 Y. Chen, J. He, H. Tian, D. Wang and Q. Yang, *J. Colloid Interface Sci.*, 2014, **428**, 1–7.
29 S. Furukawa, D. Tsukio, T. Shishido, K. Teramura and T. Tanaka, *J. Phys. Chem. C*, 2012, **116**, 12181–12186.

30 J. C. Matsubu, S. Zhang, L. DeRita, N. S. Marinkovic, J. G. Chen, G. W. Graham, X. Pan and P. Christopher, *Nat. Chem.*, 2017, **9**, 120–127.
31 V. M. Benitez, S. P. de Lima, M. do Carmo Rangel, D. Ruiz, P. Reyes and C. L. Pieck, *Catal. Today*, 2017, **289**, 53–61.
32 L. Wolski, I. Sobczak and M. Ziolek, *J. Catal.*, 2017, **354**, 100–112.
33 D. A. G. Aranda, A. L. D. Ramos, F. B. Passos and M. Schmal, *Catal. Today*, 1996, **28**, 119–125.
34 S. Guerrero, J. T. Miller and E. E. Wolf, *Appl. Catal., A*, 2007, **328**, 27–34.
35 B. Liu, H. Wang, Y. Chen, J. Wang, L. Peng and L. Li, *J. Alloys Compd.*, 2016, **682**, 584–589.
36 S. B. T. Tran, H. Choi, S. Oh and J. Y. Park, *J. Catal.*, 2019, **375**, 124–134.
37 Y. Liu, M. Tursun, H. Yu and X. Wang, *Mol. Catal.*, 2019, **464**, 22–28.
38 P. Justin, P. Hari Krishna Charan and G. Ranga Rao, *Appl. Catal., B*, 2010, **100**, 510–515.
39 P.-P. Du, X.-C. Hu, X. Wang, C. Ma, M. Du, J. Zeng, C.-J. Jia, Y.-Y. Huang and R. Si, *Inorg. Chem. Front.*, 2017, **4**, 668–674.
40 Y. Yuan, A. P. Kozlova, K. Asakura, H. Wan, K. Tsai and Y. Iwasawa, *J. Catal.*, 1997, **170**, 191–199.
41 P.-P. Du, W.-W. Wang, C.-J. Jia, Q.-S. Song, Y.-Y. Huang and R. Si, *Appl. Catal., A*, 2016, **518**, 87–101.
42 R. M. Rioux, H. Song, J. D. Hoefelmeyer, P. Yang and G. A. Somorjai, *J. Phys. Chem. B*, 2005, **109**, 2192–2202.
43 I. Nowak and M. Ziolek, *Chem. Rev.*, 1999, **99**, 3603–3624.
44 S. Y. Moon, *RSC Adv.*, 2016, **6**, 18198–18203.
45 E. O. Jardim, S. Rico-Francés, F. Coloma, J. A. Anderson, E. V. Ramos-Fernandez, J. Silvestre-Albero and A. Sepúlveda-Escribano, *Appl. Catal., A*, 2015, **492**, 201–211.
46 T. S. Mozer and F. B. Passos, *Int. J. Hydrogen Energy*, 2011, **36**, 13369–13378.